Electronic Supplementary Material (ESI) for Dalton Transactions.
This journal is © The Royal Society of Chemistry 2023

Supporting Information:

Highly porous thermoelectric composites with high figure of merit and low thermal conductivity from solution-synthesized porous $Bi_2Si_2Te_6$ nanosheets

Dabin Park[a], Minsu Kim[a] and Jooheon Kim[a,b,c]*

[a]School of Chemical Engineering & Materials Science,

Chung-Ang University, Seoul 06974, Republic of Korea

[b]Department of Advance Materials Engineering,

Chung-Ang University, Anseong 17546, Republic of Korea

[c]Department of Intelligent Energy and Industry, Graduate School,

Chung-Ang University, Seoul 06974, Republic of Korea

*Corresponding author: jooheonkim@cau.ac.kr (J. Kim)

Supporting Information Contents:

Note 1. Expeimental Methods

1.1. Materials

Bismuth (99%, Bi), powder, silicon (99%, Si), tellurium (99%, Te), dimethyl sulfoxide (DMSO, 99%. $(CH_3)_2SO$), and lithium hydroxide (98%, LiOH) were purchased from Sigma-Aldrich (St. Louis, MO). Ethylene glycol (99%, $C_2H_4(OH)_2$), hydrochloric acid (35-37%, HCl), acetone (99.8%, CH_3COCH_3) and ethanol (94.5%, C_2H_5OH) were supplied from Daejung Chemicals & Metals Co. (Seoul, Korea). PEDOT:PSS (Clevios PH 1000) was purchased from Heraus Clevios GmbH. All chemicals were used without further purification.

1.2. Preparation of $Bi_2Si_2Te_6$ NS

A $Bi_2Si_2Te_6$ ingot was prepared adopting a solid-state reaction. Briefly, stoichiometric amounts of Bi, Si, and Te were loaded into a quartz ampoule, which was then evacuated, sealed by flame, and slowly heated up to 873 K in 6 h. After keeping this temperature for 24 h, the furnace was subsequently cooled to room temperature (298 K). The prepared ingot was then ground into fine powders with an agate mortar and ball milled using zirconia balls in an inert atmosphere. Subsequently, 1 g of $Bi_2Si_2Te_6$ powder was placed into a Teflon-lined autoclave filled with a solution consisting of 200 ml of ethylene glycol and 0.8 g of LiOH. The autoclave was heated at 473 K for 48 h to achieve the intercalation of the lithium ions into the layered $Bi_2Si_2Te_6$. The solution was then allowed to cool down naturally to room temperature. The resulting product was collected by filtration, rinsed many times with acetone to eliminate the residual reactant, and then dried in a vacuum oven at 333 K for 24 h. Afterwards, 0.5 g of Li-intercalated $Bi_2Si_2Te_6$ powder was placed into a laboratory beaker filled with 200 ml of deionized (DI) water. The beaker was then sealed and sonicated at low power for 1 h. The resulting dispersions were centrifuged at 1000 rpm for 30 min and then the supernatant was

collected. Next, the supernatant was centrifuged at 8000 rpm for 30 min. The resulting powder was purified several times with 3 vol.% HCl and DI water to remove possible oxidized layers from the nanosheet surface. The final product was collected after repeatedly washing with ethanol, and then dried in a vacuum oven.

1.2. Preparation of p-BST(x) composite

After the 1h of bath sonication, additional sonication was performed in Li-BST solution using a probe sonicator (Sonics & Materials, VCX-750) to prepare b-BST composite at sonication power of 200W and various times (1, 2, 3, 4, and 6 h). During operation, there was a 1 s pause once every 3 s to prevent overheat of solution. After ultrasonication, the final product was centrifuged and washed with DI water and ethanol, and then dried in a vacuum oven. The final product was loaded into a Fe mold and pressed at 200 ˚C under a pressure of 100 MPa for 5 minutes.

1.3. Characterization

X-ray diffraction (XRD, New D8 Advance, Bruker AXS) was used to characterize the crystal structures of the synthesized materials. XRD was performed at 40 mA, 40 kV, and a scan rate of 1°/s, with 2θ ranging from 5° to 70° using Cu Kα radiation (λ = 0.154056 nm). The binding energy peaks of the synthesized materials were investigated with X-ray photoelectron spectroscopy (XPS, VG-Microtech, ESCA2000). The microstructure was observed with field-emission scanning electron spectroscopy (FE-SEM, SIGMA), field-emission transmission microscopy (FE-TEM, JEM-2100F). Elemental mappings of the samples were analyzed by energy-dispersive X-ray spectroscopy (EDS, NORAN system 7, Thermo Scientific). Thermogravimetric analysis (TGA, TGA-2050, TA Instrument) was performed in a N_2

atmosphere.

The charge carrier concentration (n) and mobility (μ) were measured using Hall-effect measurements (HMS-300, Ecopia). The electrical conductivity and Seebeck coefficient were investigated using an Ulvac Riko ZEM-3 instrument under a helium atmosphere. All thermoelectric properties of samples were measured with in-plane. Five replicates of the composite samples were used for each test to verify the reproducibility of the experiments.

The charge carrier concentration (n) and mobility (μ) were measured using Hall-effect measurements (HMS-300, Ecopia). The electrical conductivity and Seebeck coefficient were investigated using an Ulvac Riko ZEM-3 instrument under a helium atmosphere. The thermal conductivity of the composites was calculated from the relation $\kappa = C_p \cdot \alpha \cdot \rho$, where C_p, α, and ρ are the specific heat, thermal diffusivity, and bulk density of the composite, respectively. The laser flash analysis (LFA, Netzsch Instruments Co., NanoFlash LFA 467) method was employed to measure the room-temperature thermal diffusivity. All thermoelectric properties of samples were measured with in-plane. Five replicates of the composite samples were used for each test to verify the reproducibility of the experiments.

2. Figures

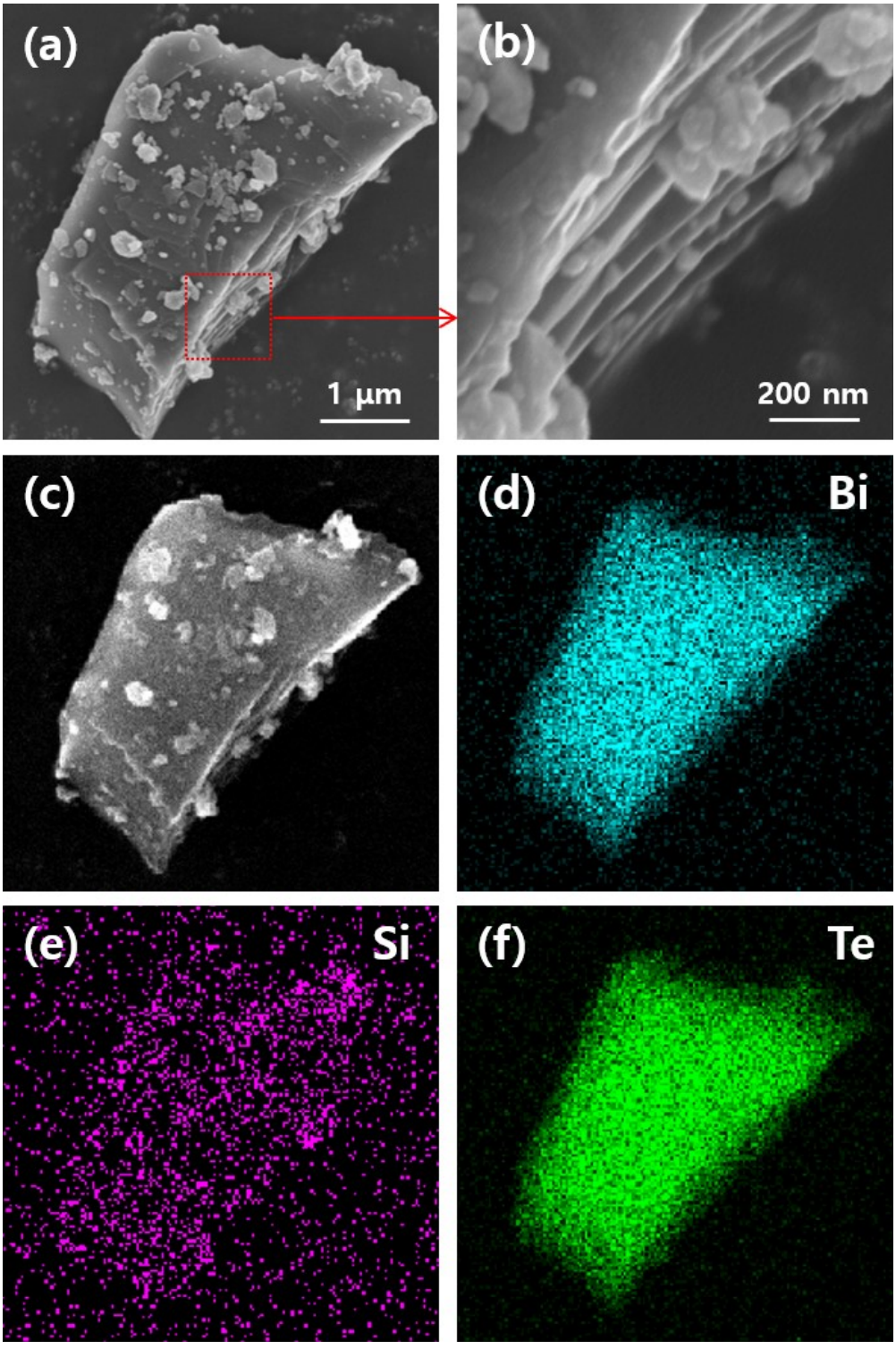

Fig. S1. (a) low- and (b) high-magnification FE-SEM images of BST ingot. FE-SEM image and the corresponding EDS mapping images of (c) BST ingot (d-f) corresponding EDS mapping images of $Bi_2Si_2Te_6$ ingot.

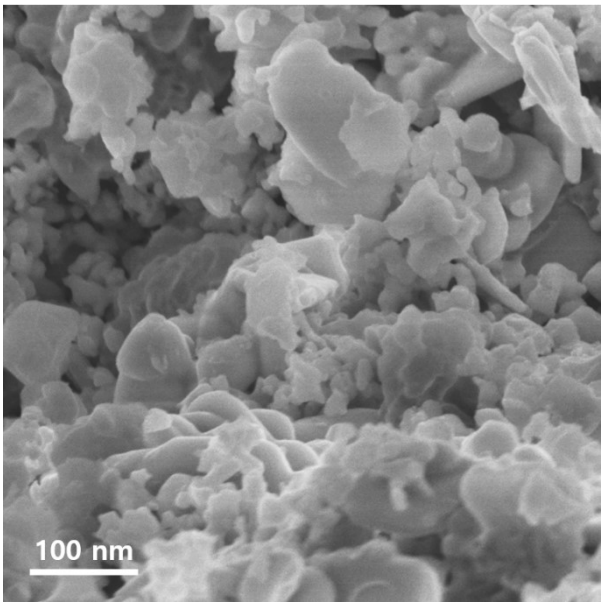

Fig. S2. FE-SEM image of pellet for the p-BST(2) after the hot pressing.

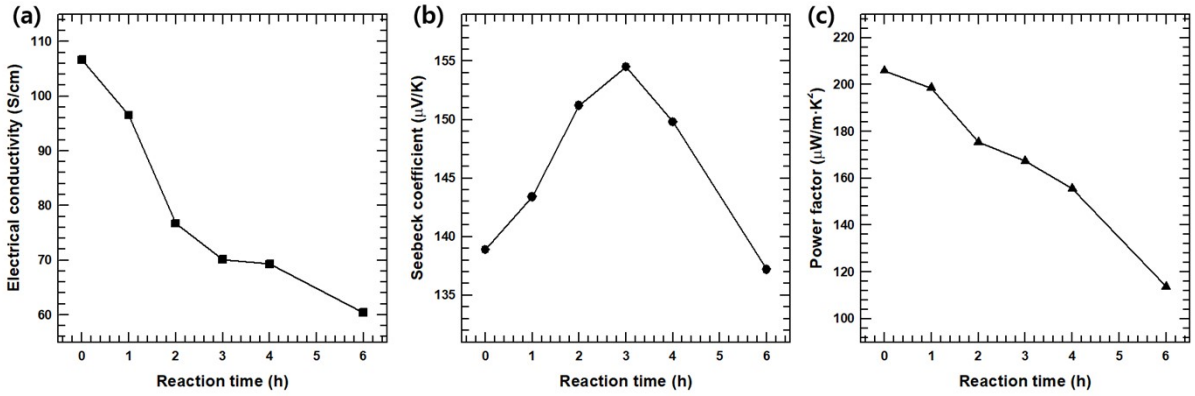

Fig. S3. (a) Electrical conductivity, (b) Seebeck coefficient, (c) power factor of p-BST(x) composites with various reaction times.

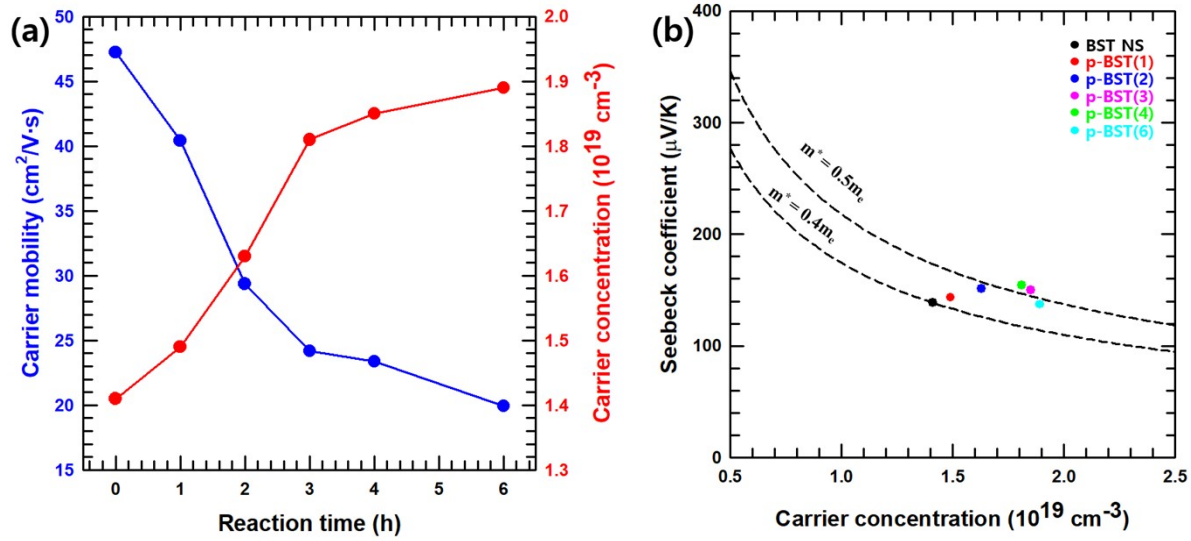

Fig. S4. (a) Carrier concentration and mobility values of p-BST(x) composite with different reaction times. (b) Seebeck coefficiet *S versus* carrier concentration of the p-BST(x) composites. Dashed line are the calurated Pisarenko plot for various effective mass as indicated.

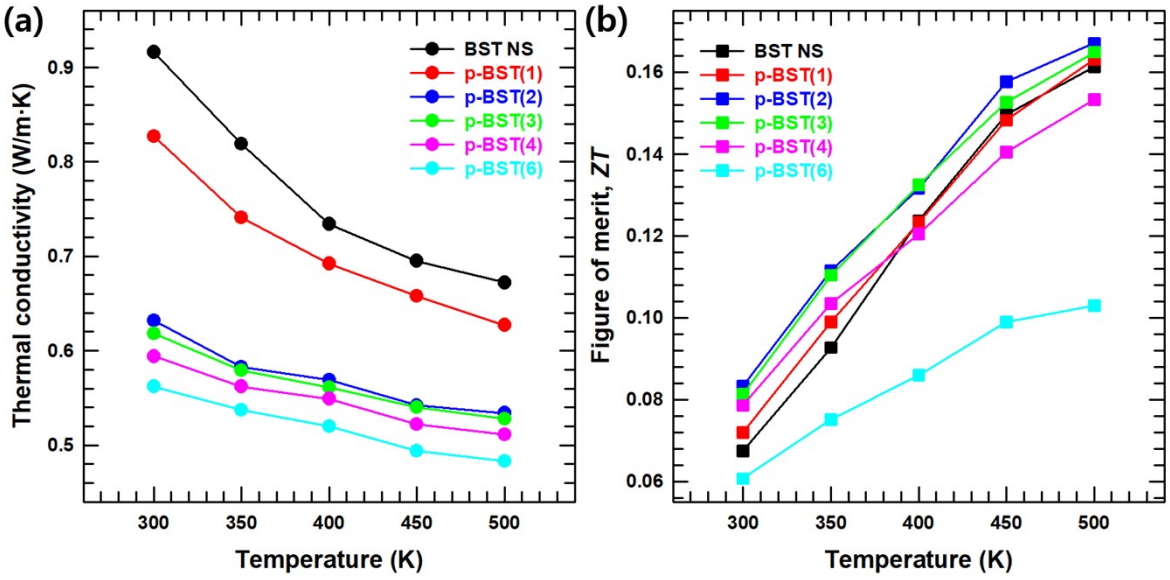

Fig. S5. Temperature dependent (a) Thermal conductivity, and (b) ZT values of p-BST(x) composite.

	$Bi_2Si_2Te_6$	p-BST(1)	p-BST(2)	p-BST(3)	p-BST(4)	p-BST(6)
Powder	5.81	5.54	4.77	4.68	4.36	4.03
Hot-pressed	6.24	5.88	5.36	5.22	4.99	4.67

Table S1. Density values of powder and sintered p-BST composite with different reaction times.

	$Bi_2Si_2Te_6$	p-BST(1)	p-BST(2)	p-BST(3)	p-BST(4)	p-BST(6)
Lorenz number ($10^{-8}W/\Omega \cdot K^2$)	~1.802	~1.890	~1.772	~1.764	~1.775	~1.806

Table S2. Variation in the calculated *L* of the SPS BST with various reaction times

Composites	κ (W/m·K)	Temperature (K)	References
Porous $Bi_2Si_2Te_6$	~0.56	~300	This study
$Bi_2Si_2Te_6$	~0.7	670	1
$Bi_{2-x}Pb_xSi_2Te_6$	~0.57	773	2
$Bi_{2-x}Sb_xSi_2Te_6$	~0.62	623	3

Table S3. The lowest total thermal conductivity (κ) of various $Bi_2Si_2Te_6$-based composites.

References

1. H. Jang, S. Abbey, B. Frimpong, C. V. Nguyen, P. Ziolkowski, G. Oppitz, M. Kim, J. Y. Song, H. S. Shin and Y. S. Jung, *ACS Appl. Mater. Interfaces*, 2022, **14**, 1270-1279.
2. Y. Luo, Z. Ma, S. Hao, S. Cai, Z.-Z. Luo, C. Wolverton, V. P. Dravid, J. Yang, Q. Yan and M. G. Kanatzidis, *J. Am. Chem. Soc.*, 2022, **144**, 1445-1454.
3. C. Chen, D. Shen, C. Xia, Z. Zhang, W. Wang, Q. Zhang and Y. Chen, *Chem. Eng. J.*, 2022, **441**, 135968.